NUMERICAL MODELING OF VORTEX STRUCTURES UNDER A BROKEN SOLITARY WAVE USING SMOOTHED PARTICLE HYDRODYNAMICS METHOD

Rozita Jalali Farahani[1], Robert A. Dalrymple[2]

Water wave breaking and the resulting surf-zone turbulence play a role in sediment transport, wave damping, and mixing processes. The vortex structures associated with wave breaking carry large amount of turbulent momentum and turbulent kinetic energy and therefore have a crucial effect on the safety of vessels and structures located in the surf zone. In this study, turbulent vortical structures under a broken solitary wave is studied using a three-dimensional Smoothed Particle Hydrodynamics (SPH) method. A broken solitary wave is of interest since the generation and evolution of the three-dimensional vortex structures under a broken wave can be isolated from the case of a periodic wave train, which has undertow and residual turbulence induced from previously broken waves. Further, a solitary wave is a first approximation to a tsunami wave. The numerical model predicts water surface evolution very well in comparison with the experimental results of Ting (2006). The numerical results show organized coherent structures trailing the wave and characterized by reversed horseshoe (hairpin) vortices, traveling downward, which appear to be the previously found obliquely descending eddies. These horseshoe coherent structures transport momentum and turbulent kinetic energy downward into the water column and likely have a significant role in bed and beach erosion. Different terms of vorticity equations are studied and it is concluded that vortex stretching and vortex bending play an important role on the generation and evolution of reversed horseshoe structures.

Keywords: Solitary wave; Obliquely descending eddies; Smoothed Particle Hydrodynamics

INTRODUCTION

As waves propagate towards nearshore regions and break, an intensive turbulence is generated, which plays a crucial role in sediment transport, wave damping, mixing processes, and thermal diffusion within the underlying flow field. Investigation of the turbulence under breaking wave can give a better understanding of wave dynamics in the nearshore regions and the resulting vortex structures. In addition, the vortex structures and rotations associated to the water wave breaking can have a dominant effect on the safety of vessels and structures located in the coastal regions.

The wave dynamics and resulting turbulence have been mostly studied by two dimensional numerical models. Lin and Liu (1998) performed a two dimensional RANS numerical model to study the wave propagation and breaking in the surf zone. They found a 'roller' region in the breaking wave front and reported it as a source region of turbulence generation. Watanabe et al. (1999) used large-eddy simulation (LES) method to study the structure of turbulence flow field under spilling and plunging breakers. They reported characteristic structure of large-scale eddies under broken waves and referred to them as 'horizontal eddies' and 'obliquely descending eddies'. Christensen (2006) also performed LES method to model spilling and plunging breakers. The order of magnitude of the turbulent energy in the numerical results was found to be in agreement with experimental results. As the waves break, three dimensional turbulence and vortex structures are generated within the flow field beneath the broken waves. Hence a three-dimensional numerical method can lead to a better understanding of the generation mechanism of large-scale eddies under broken waves.

In this study three-dimensional Smoothed Particle Hydrodynamics (SPH) numerical method is used to investigate broken solitary waves dynamics within the surf zone and the turbulence structure within the underlying flow field. SPH is a Lagrangian, mesh-free particle method, which was first introduced by Gingold and Monaghan (1977) to solve gas dynamical problems of astronomical interest. SPH has been used to model a vast range of problems including fluid mechanics problems and was shown to be capable of modeling flows with complicated surface deformations. Monaghan (1994) modeled a dam-break problem as well as water waves using SPH and the Navier-Stokes equations. Monaghan and Kos (1999) continued their researches on solitary waves in the surf zone and Scott Russell's wave generation using SPH method. Other wave-related studies using SPH numerical method include breaking waves (Monaghan et al., 2003), impact of wave on structures (Dalrymple et al., 2002; Gómez-Gesteira and Dalrymple, 2004), and waves in the surf zone (Dalrymple and Rogers, 2006).

Water waves breaking in the surf zone was also investigated in various experimental studies. Nadaoka et al. (1989) performed an experimental study in a 0.6 m deep, 0.4 m wide, and 20 m long wave channel,

[1]rozita@jhu.edu, Department of Civil Engineering, Johns Hopkins University, USA
[2]rad@jhu.edu, Department of Civil Engineering, Johns Hopkins University, USA

equipped with a flap-type wave generator. They investigated periodic spilling waves breaking on a plane beach and found two-dimensional large-scale spanwise vortex structures under breaking waves with axes parallel to the crest line. They also found three-dimensional large-scale vortex structures behind the broken waves and called them obliquely descending eddies. The three-dimensionality of the flow structure behind the wave crest, was visualized using air bubbles. Ting and Kirby (1994) conducted a series of experiments regarding the turbulence structure under plunging and spilling breakers and compared the results with each other. Experimental results revealed that the turbulent kinetic energy is transported landward under a plunging breaker and is dissipated within one wave cycle, whereas the turbulent kinetic energy is transported seaward under a spilling breaker and the dissipation rate is much slower.

In this study, three-dimensional SPH numerical method is used to model a spilling solitary wave. The three-dimensional vortex structures under the broken waves and their generation mechanism are also investigated

SPH NUMERICAL METHOD AND GPUSPH MODEL

SPH numerical method

SPH was developed as mesh-based methods were found to be problematic for problems with large deformations and lack of defined boundaries. SPH numerical method is a Lagrangian method where a kernel approximation is used to represent the integral form of the governing equations. The partial differential equations (PDEs) are converted to ordinary differential equations (ODEs) in discretized form with respect to time only. The ODEs are then solved using an integration algorithm for each time step and the field variables including velocities and positions are computed.

The kernel function that is used in our study is called Wendland kernel function and has the advantage of being based on one algebraic equation and having a compact support.

$$W(q,h) = \alpha_D \begin{cases} (1-\frac{q}{2})^4(1+2q) & 0 \le q \le 2; \\ 0 & q > 2. \end{cases} \tag{1}$$

The parameter h is the smoothing length of the kernel function, which indicates the support domain of the kernel function. q is equal to r/h, where r is the distance between two particles. α_D is equal to $3/(4h)$, $7/(4\pi h^2)$ and $21/(16\pi h^3)$ for one, two and three dimensional space respectively.

The governing equations that are solved to model the water waves are conservation of mass equation and conservation of momentum equation. The differential form of the conservation of mass equation is given as:

$$\frac{\partial \rho}{\partial t} + \rho(\nabla.\vec{u}) = 0 \tag{2}$$

where ρ is density, $\vec{u}$ is velocity, and t is time. The SPH form of conservation of mass equation can be written as:

$$\begin{aligned} \frac{\partial \rho_a}{\partial t} &= -\sum_b m_b \vec{u}_b \nabla_a W(r_{ab}) + \vec{u}_a \sum_b m_b \nabla_a W(r_{ab}) \\ &= \sum_b m_b (\vec{u}_a - \vec{u}_b) \nabla_a W(r_{ab}) \end{aligned} \tag{3}$$

where a is the particle of interest, b is the neighboring particle, and m is the particle mass. The differential form of the momentum equation is given as:

$$\frac{D\vec{u}}{Dt} = -\frac{1}{\rho}\nabla P + \vec{g} + \vec{\Theta} \tag{4}$$

The first term on the right hand side of the above equation is the pressure gradient term that can be written in SPH form as:

$$-\sum_b (\frac{P_a}{\rho_a^2} + \frac{P_b}{\rho_b^2}) m_b \nabla_a W(r_{ab}) \tag{5}$$

The second term on the right hand side of the equation (4) is the gravitational acceleration, which is defined as: $\vec{g} = (0, 0, 9.81)\frac{m}{s^2}$. The third term on the right hand side of the equation (4) is the viscous term. The effect of turbulence is considered in the SPH method using a model similar to the Sub-Grid Scale (SGS) turbulence model in the Large Eddy Simulation (LES) method (Dalrymple and Rogers, 2006). SPH form of turbulent shear stress term of momentum equation can discretized as:

$$\frac{1}{\rho}\nabla.\tau_{ab}|_a = \sum_b m_b(\frac{\tau_{ab}|_a}{\rho_a^2} + \frac{\tau_{ab}|_b}{\rho_b^2}).\nabla_a W_{ab} \tag{6}$$

where summation is made within the neighboring particles of the particle of interest. In our study we used the SPS approach of Dalrymple and Rogers, (2006) with constant Smagorinsky coefficient. In weakly compressible SPH, the fluid is assumed to be weakly compressible, with a very small density fluctuations. This assumption allows the pressure to be calculated from an equation of state as (Monaghan and Kos, 1999):

$$P = \beta[(\frac{\rho}{\rho_0})^\gamma - 1] \tag{7}$$

where ρ_0 is the initial density, γ is chosen to be equal to 7, and parameter β is calculated as:

$$\beta = \frac{\rho_0 c^2}{\gamma} \tag{8}$$

GPUSPH model

Previously, parallel computations were mostly performed using multiple Central Processing Units (CPUs). Recent advances in computer technology permit the use of Graphics Processing Units (GPUs) for parallel computing with high computational power and low expenses. Three-dimensional SPH is computationally intensive and it has a data-parallel nature. On the other hand, the GPU cards have parallel structures. Therefore, the three-dimensional SPH method performs very well on GPU cards. In 2007, a new GPU parallel architecture is introduced as Compute Unified Device Architecture (CUDA), which uses high-level languages such as C, C++, and Fortran to program the graphic cards.

GPUSPH is an open source package that performs the massive computations of Smoothed Particle Hydrodynamics method on Nvidia graphic cards for various applications. GPUSPH was started by Alexis Hérault (Hérault et al. 2010) in a study of lava cooling. It uses CUDA language and was inspired by the Nvidia SDK program Particles (*http : //www.ce.jhu.edu/dalrymple/GPUSPH/Home.html*). GPUSPH is also capable of illustrating real-time images of fluid parameters such as velocity and pressure. GPUSPH is written in an object-oriented platform and consists of several interacting objects. Therefore, new features or physical problems can be easily added to the existing platform. For the wave-related numerical modeling, a couple of additional features are added to the existing package (Farahani et al., 2014). Using these features, fluid parameters at Eulerian nodes can be observed as well as Lagrangian particles, which leads to a better comparison between numerical SPH results and Eulerian experimental results. In addition, free-surface particles can be detected at each time step, which makes the calculations of mean parameters possible.

THREE-DIMENSIONAL VORTEX STRUCTURES UNDER A BROKEN SOLITARY WAVE

wave tank set-up

Different types of large-scale vortex structures under a broken solitary wave are investigated using the three-dimensional SPH method. The wave tank used in the numerical study is 25 m long, 0.9 m wide and is located on a 1 in 50 plane slope. The wave tank set-up was inspired by the solitary wave experiments of Ting (2006). A solitary wave of 0.22 m height is generated using a piston type wave generator. The water depth at the location of the wave generation is equal to 0.3 m. Figure 1 illustrates the wave tank set-up.

The Goring and Raichlen (1980) approach is used to generate the waves. The basic concept is to match the velocity of the wave generator to the corresponding depth-averaged velocity of the water particles.The generation equation for solitary wave is defined as:

$$\frac{\zeta(t)}{S} = \frac{1}{2}\{1 + \tanh 2[(3.8 + \frac{H}{h})(\frac{t}{\tau} - \frac{1}{2}) - \frac{H}{h}(\frac{\zeta}{S} - \frac{1}{2})]\} \tag{9}$$

where ζ is the wave generator displacement, S is the stroke, H is the wave height, h is the water depth, and τ is the duration of wave generator motion.

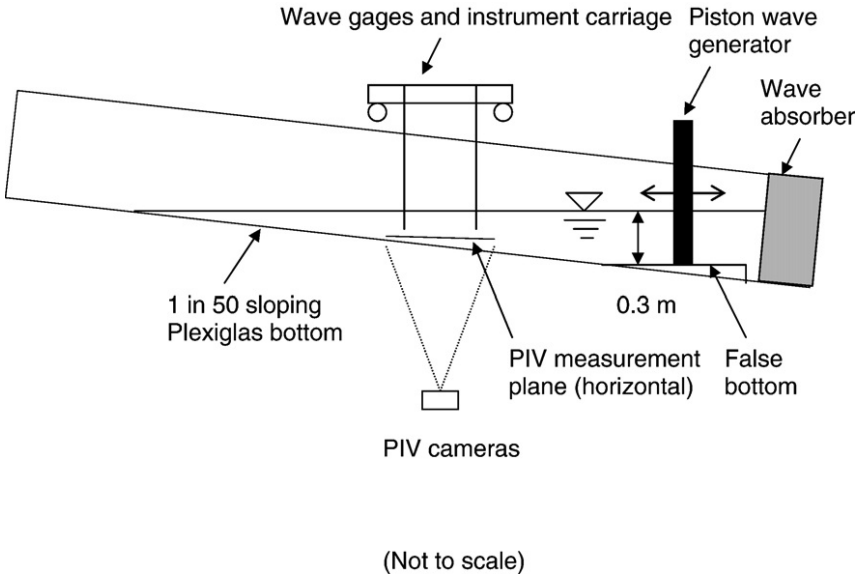

Figure 1: Schematic plot of experimental set-up (Ting, 2006)

Numerical results

Numerical results of spilling solitary wave is compared to the experimental results. The wave heights were measured at 12 stations between the wave generator and the still water shoreline. The distance between adjacent stations was 1 m. Figure 2 illustrates the ensemble-averaged water surface profile in both experimental measurements and numerical simulation.

Figure 3 illustrates the numerical results as well as the experimental results of ensemble-averaged horizontal velocity under the solitary wave. In this figure the numerical time = 3.5 s is equal to the experimental time = 34 s. The instantaneous velocity is decomposed to ensemble averaged velocity and the turbulent velocity as:

$$\vec{u} = <\vec{u}> + \vec{u}' \tag{10}$$

The coherent vortex structures are detected using λ_2 criterion (Jeong and Hussain, 1994). In this method, the tensor $S^2 + \Omega^2$ is calculated where S and Ω are the symmetric and antisymmetric components of velocity gradient tensor $\nabla\vec{u}$. The term λ_2 is obtained as the second largest eigenvalue of this tensor and a vortex core is defined as a region with a negative λ_2 threshold. Figure 4 illustrates the coherent structures detected by λ_2 criterion at t=5.5 s of the numerical simulation.In this figure, a reversed horseshoe vortex structure can be observed at the position of the measurement location.

GENERATION OF 3D VORTEX STRUCTURES

Horseshoe (hairpin) vortex structures

A coherent structure is defined as “A connected turbulent fluid mass with instantaneously phase-correlated vorticity over its spatial extent" (Hussain, 1986). The coherent structures play an important role in the transport of mass, momentum, and heat. In our study, different types of coherent vortex structures are observed and studied. Spanwise vortex structures are developed at the wave toe where the wave front hits the water surface. Vertical vortex structures are observed at the tow of the broken wave. After a short period of time, reversed horseshoe structures begin to develop and travel downward towards the bed bottom.These structures are initiated from the portions of the spanwise roller where the curvature is relatively high. Two legs of the reversed horseshoe structures have counter-rotating vorticities that were previously observed as obliquely descending eddies and were assumed to be two separate vortex structures (Nadaoka et al., 1989). In addition to reversed horseshoe vortices, there exist quasi-streamwise vortices that are primarily in streamwise direction. Figure 5 illustrates the time history of the generation and evolution of reversed horseshoe structures. The vortex structures are detected by the isosurface of $\lambda_2 = -50$.

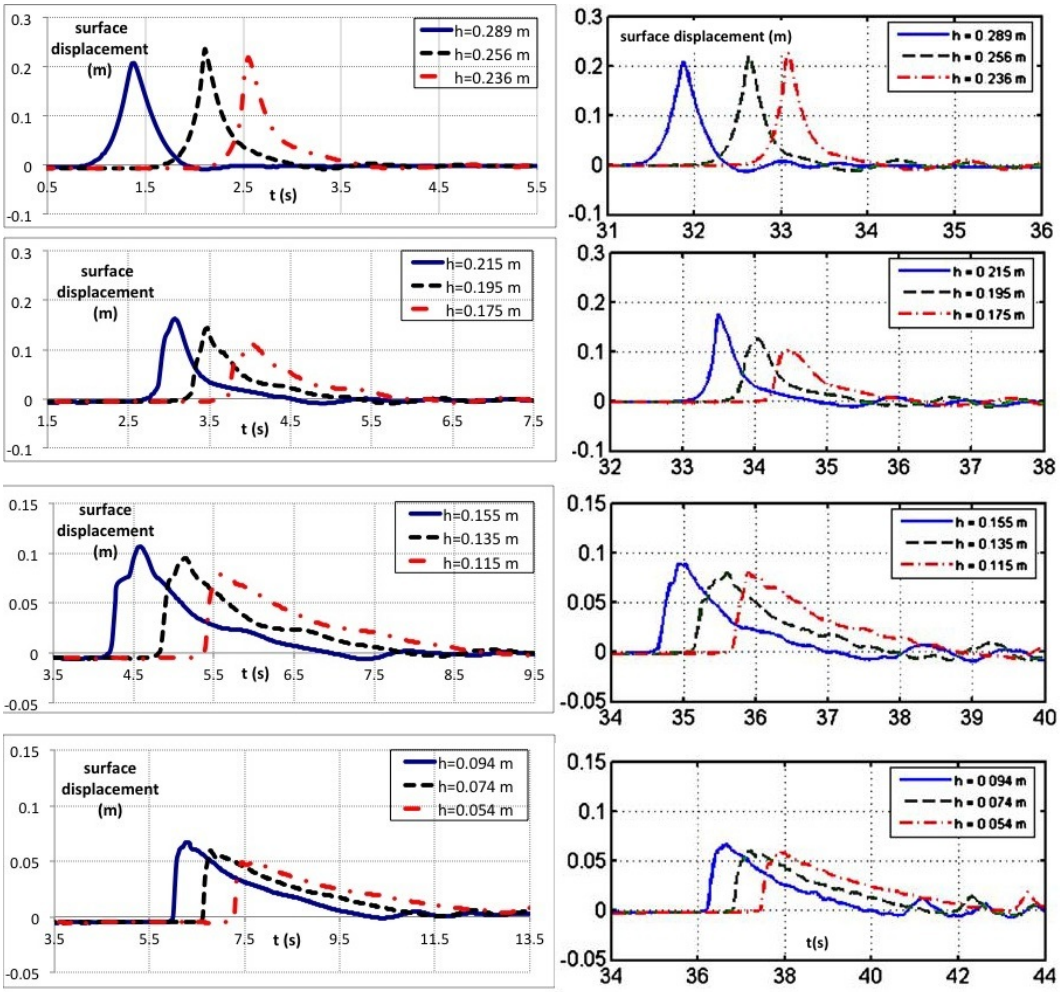

Figure 2: Ensembled-averaged wave elevations (Left: Numerical results, Right: Experimental results) - note: The time = 0.5 s of numerical results is equivalent to time = 31 s of experimental results

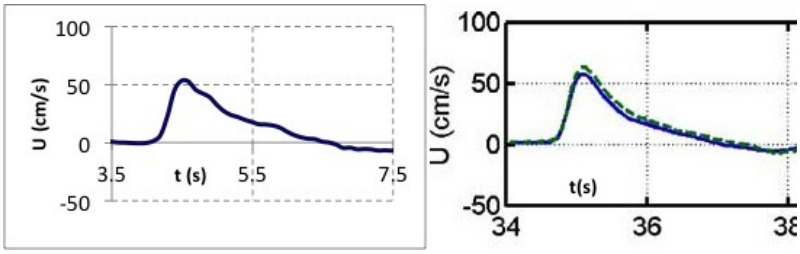

Figure 3: Four seconds of ensembled-averaged horizontal velocity under the solitary wave (Left: Numerical result; Right: Experimental result) - note: The dash line in the experimental results corresponds to the ADV measurements and the solid line corresponds to the PIV measurements. The time = 3.5 s of numerical results is equivalent to time = 34 s of experimental results

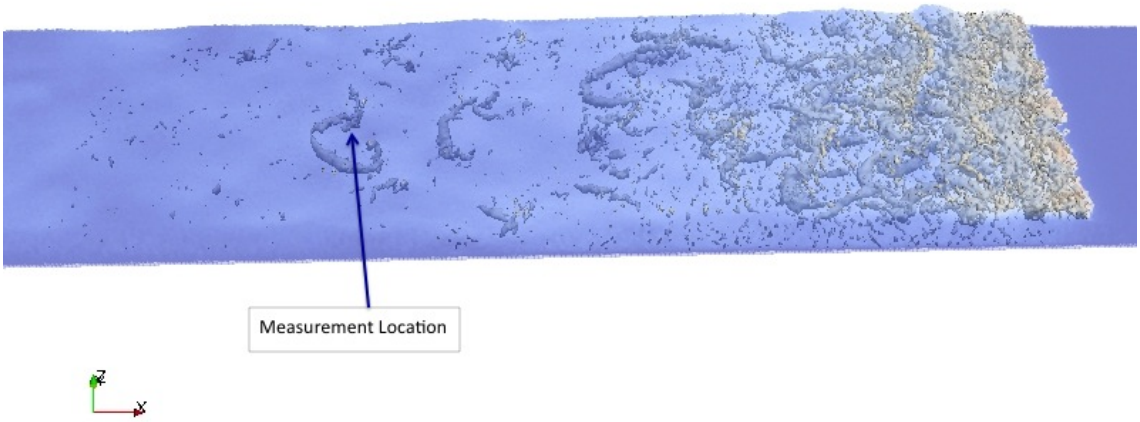

Figure 4: Vortex structures identified by the isosurface of $\lambda_2 = -25$ at numerical time=5.5 s

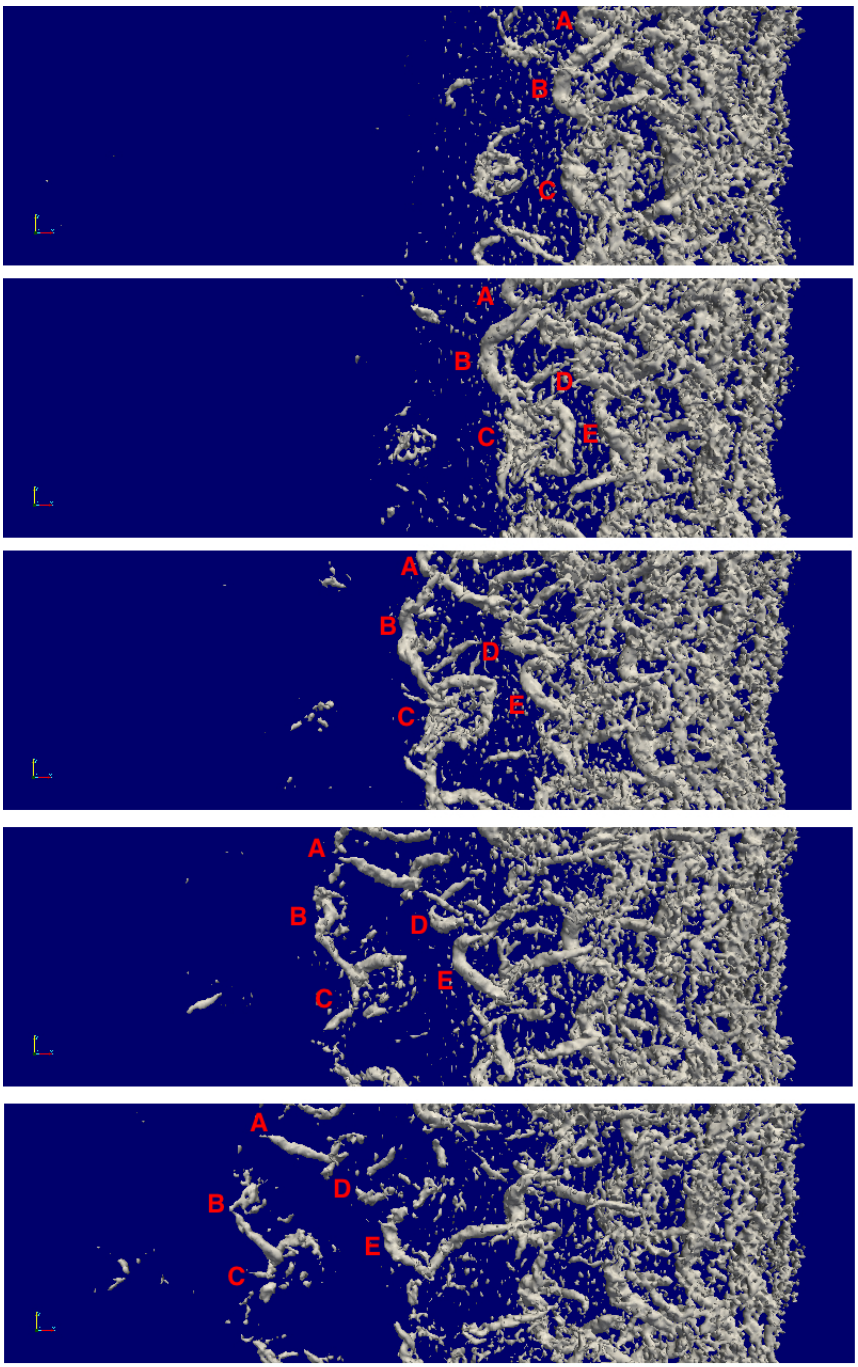

Figure 5: Vortex evolution after the broken wave at time = 3.5, 3.7, 3.9, 4.1, 4.3, 4.5, 4.7, 4.9, 5.1, 5.3, 5.5s. The flow field is observed from above in a wave-following frame of reference.The vortex structures are detected by the isosurface of $\lambda_2 = -50$.

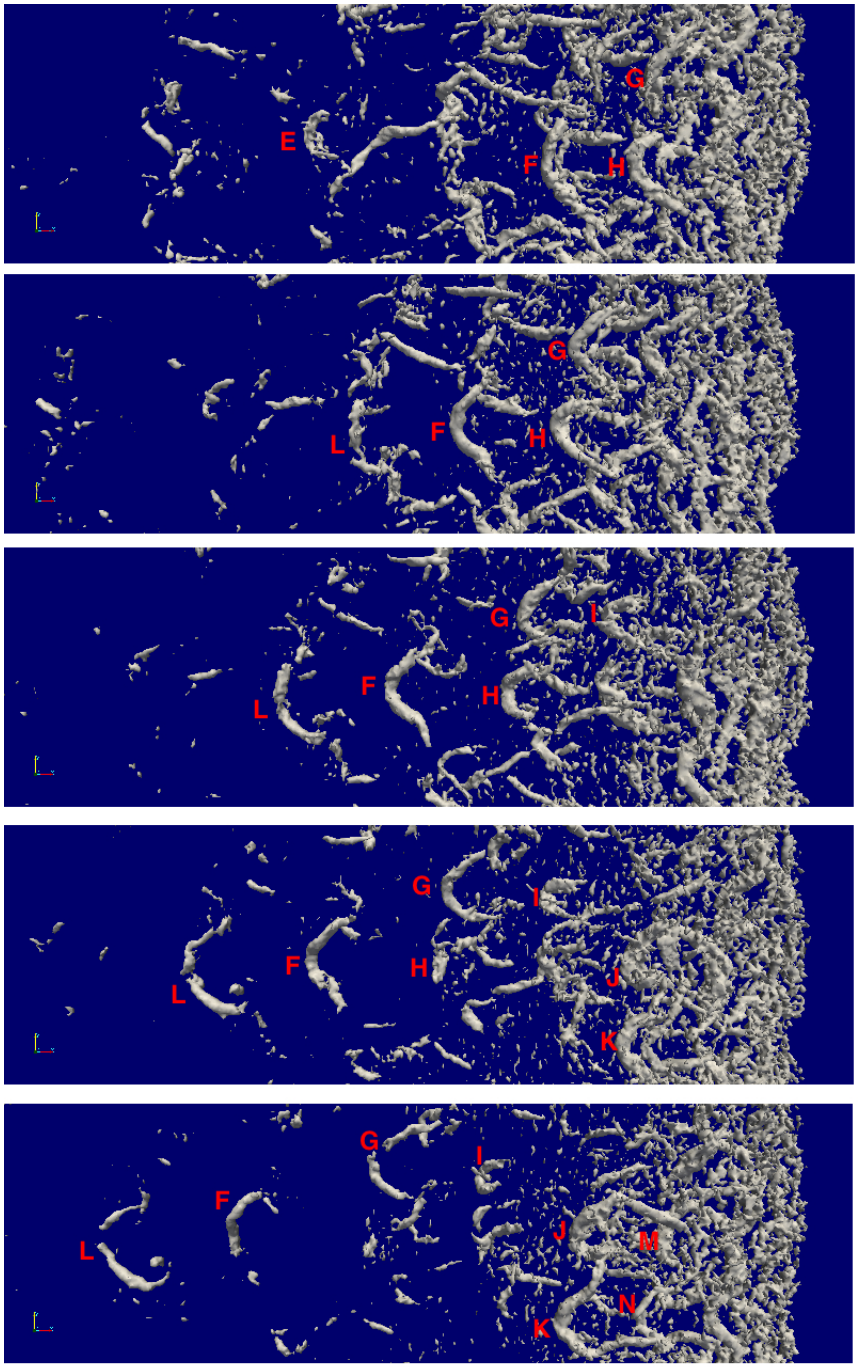

Figure 5: (Continued)Vortex evolution after the broken wave at time = 3.5, 3.7, 3.9, 4.1, 4.3, 4.5, 4.7, 4.9, 5.1, 5.3, 5.5s. The flow field is observed from above in a wave-following frame of reference.The vortex structures are detected by the isosurface of $\lambda_2 = -50$.

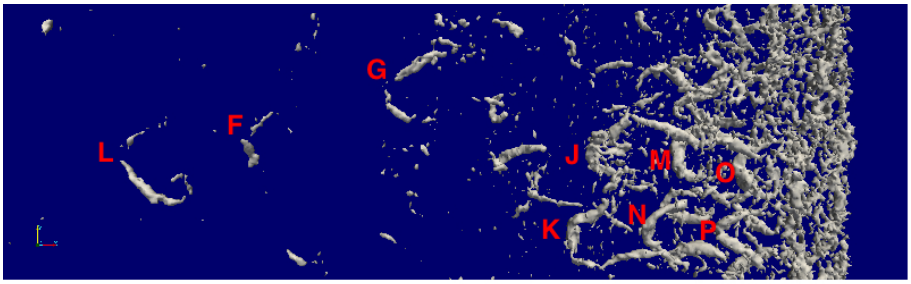

Figure 5: (Continued)Vortex evolution after the broken wave at time = 3.5, 3.7, 3.9, 4.1, 4.3, 4.5, 4.7, 4.9, 5.1, 5.3, 5.5s. The flow field is observed from above in a wave-following frame of reference.The vortex structures are detected by the isosurface of $\lambda_2 = -50$.

At time = 3.5 s, three reversed horseshoe structures (A, B, C) are initiated from the first horizontal roller. At time = 3.7 s, another two reversed horseshoe structures (D, E) are generated from the second horizontal roller. As time passes by, these structures evolve and propagate in -x-direction (from right to left) in the wave-following frame of reference. Some of the reversed horseshoe structures undergo tearing or pairing (vortex structure A, tears up at time = 4.1 s). New horseshoe structures are generated at time = 4.5 s (F, G, H), time = 4.9 s (I, L), time = 5.1 (J,K), time = 5.3 s (M,N), and time = 5.5 s (O,P).

Reynolds shear stresses and the turbulent momentum flux

Figure 6 presents the vortex structures behind the broken wave at time = 4.7 s and the resulting turbulent velocity and turbulent momentum flux. One of the reversed horseshoe structures (vortex H in figure 5) is selected and turbulent velocities (v', 'w'), streamwise vorticity (ω_x), turbulent momentum flux ($-u'w'$), and kinetic turbulent energy ($k = (u'^2 + v'^2 + w'^2)/2$) are computed. Large amount of turbulent momentum flux and turbulent kinetic energy are generated at the middle of the two counter-rotating legs and at the outer corner of the legs. The results are consistent with Kim and Moin (1986) and Yang and Shen(2009) results.

GENERATION OF THE VORTEX STRUCTURES

In this section, the generation mechanism of vortex structures including obliquely horseshoe structures (obliquely descending eddies) under broken water waves is discussed. Obliquely horseshoe structures contain both vertical and spanwise vorticities. The vorticity equations can be written as:

$$\frac{D\omega_x}{Dt} = \underbrace{\omega_x \frac{\partial u}{\partial x}}_{\text{Term one}} + \underbrace{\omega_y \frac{\partial u}{\partial y}}_{\text{Term two}} + \underbrace{\omega_z \frac{\partial u}{\partial z}}_{\text{Term three}} \tag{11}$$

$$\frac{D\omega_z}{Dt} = \underbrace{\omega_x \frac{\partial w}{\partial x}}_{\text{Term one}} + \underbrace{\omega_y \frac{\partial w}{\partial y}}_{\text{Term two}} + \underbrace{\omega_z \frac{\partial w}{\partial z}}_{\text{Term three}} \tag{12}$$

where ω_x, ω_y, and ω_z are the vorticity in x, y, and z directions. Term one of equation 11 is associated to the vortex stretching of streamwise vorticity ω_x. Term two and three of equation 11 are associated to vortex turning from spanwise vorticity ω_y and vertical vorticity ω_z to streamwise vorticity ω_x. Similarly, term one and two of equation 12 correspond to vortex turning and term three corresponds to the vortex stretching.

Figure 7 illustrates the variation of vertical velocity over the width of the tank, on a plane that is parallel to the x-y plane, at the position of $z = 0.42m$, and at time = 4 s. From this figure, one can note that the vertical velocity over the width of the tank $\frac{\partial w}{\partial y}$) has non-zero values at the head of the broken wave.

When the spilling wave breaks, spanwise vorticity (ω_y) has a nonzero value. Therefore term two of equation 12 ($\omega_y \frac{\partial w}{\partial y}$) will have a nonzero value at the locations where $\frac{\partial w}{\partial y}$ has non-zero value. Therefore, positive and negative components of vertical vorticity (ω_z) will be produced at those locations (left hand side of equation 12). In other words, spanwise vorticity turns to vertical vorticity at the positions of nonzero $\frac{\partial w}{\partial y}$. When vertical vorticity is produced, term three of equation 11 ($\omega_z \frac{\partial u}{\partial z}$) will have a nonzero value at the locations where $\frac{\partial u}{\partial z}$ has value. Figure 8 presents the velocity vectors and velocity magnitude under the broken wave.

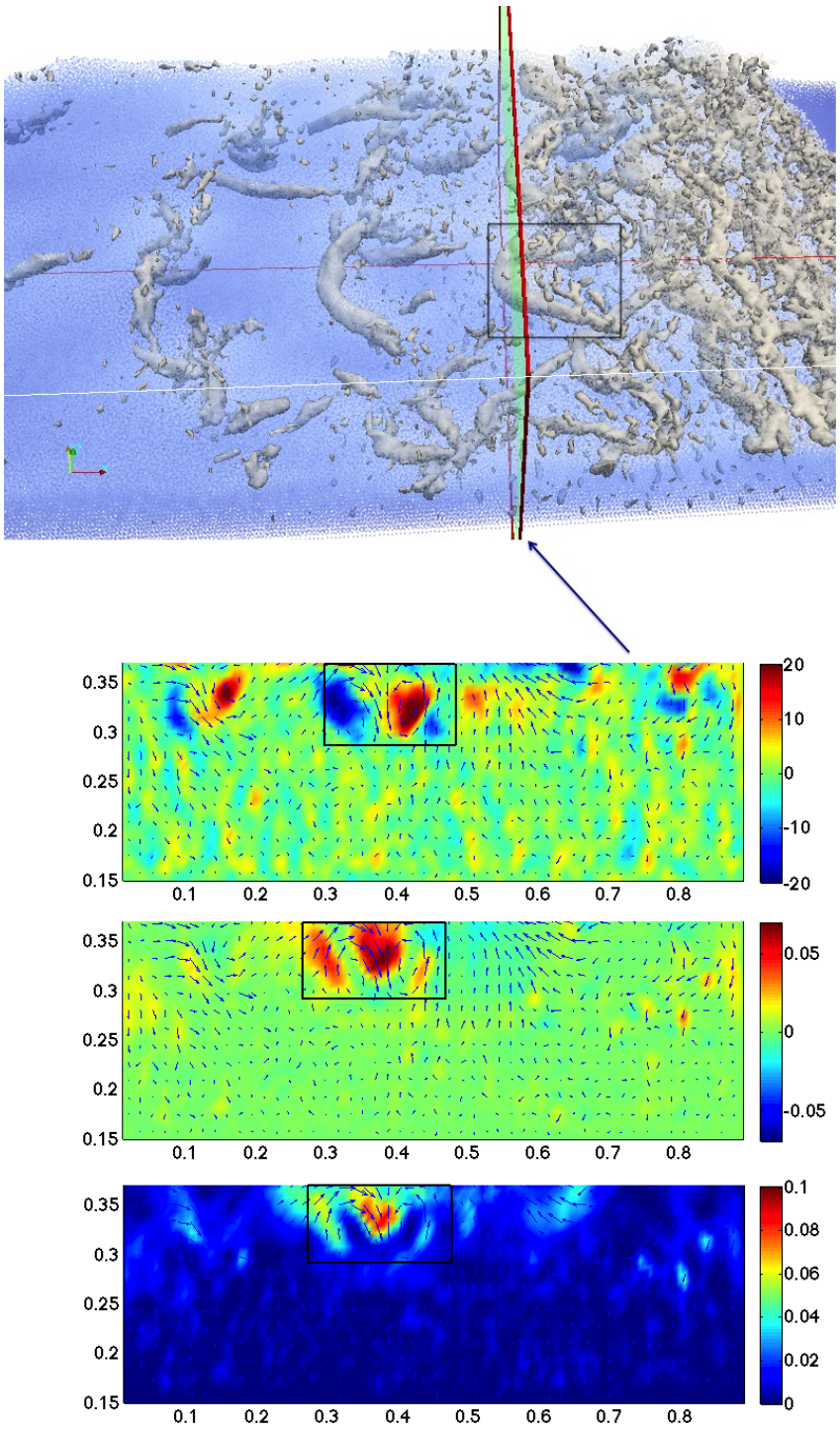

Figure 6: Reversed horseshoe structures at time = 4.7 s. From top to bottom: (a) Streamwise vorticity profile (ω_x) and turbulent velocity vectors (v', w'), (b) turbulent momentum flux ($-u'w'$), (c) Turbulent kinetic energy

Vertical gradient of streamwise velocity ($\frac{\partial u}{\partial z}$) has nonzero value beneath the broken wave. Term two of equation 11 ($\omega_y \frac{\partial u}{\partial y}$) will have a nonzero value at the locations where $\frac{\partial u}{\partial y}$ has value. Figure 9 illustrates the

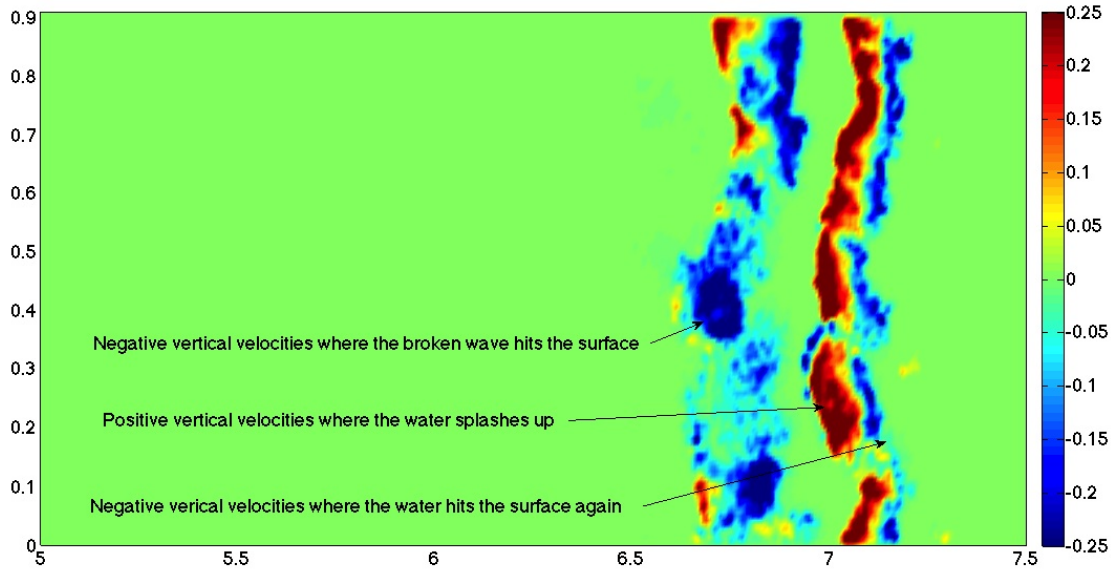

Figure 7: Vertical velocity on a plane that is parallel to the x-y plane, at the position of $z = 0.42m$, and at time = 4 s, showing the variation of vertical velocity over the width of the tank

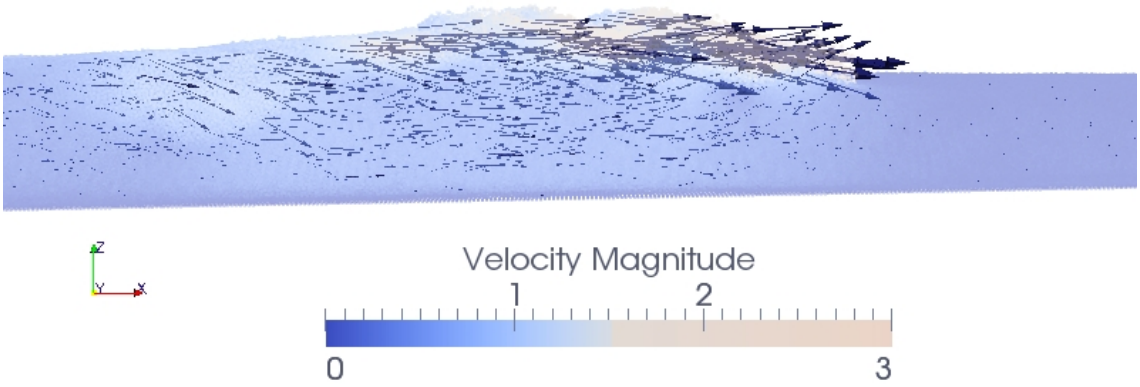

Figure 8: Velocity vectors and velocity magnitude under the broken wave

variation of streamwise velocity over the width of the tank, on a plane that is parallel to the x-y plane, at the position of $z = 0.42m$, and at time = 4 s. In equation 11 , both term two and three have nonzero values and contribute in the generation of spanwise vorticity ω_x (left hand side of equation 11).

The vorticity equation terms have been calculated separately to study the importance of each term. Figure 10 presents the different terms of equation 11 and 12. Terms two and three of equation 11 ($\omega_y \frac{\partial u}{\partial y}$, $\omega_z \frac{\partial u}{\partial z}$) are the largest and are associated to vortex turning from spanwise vorticity to streamwise vorticity

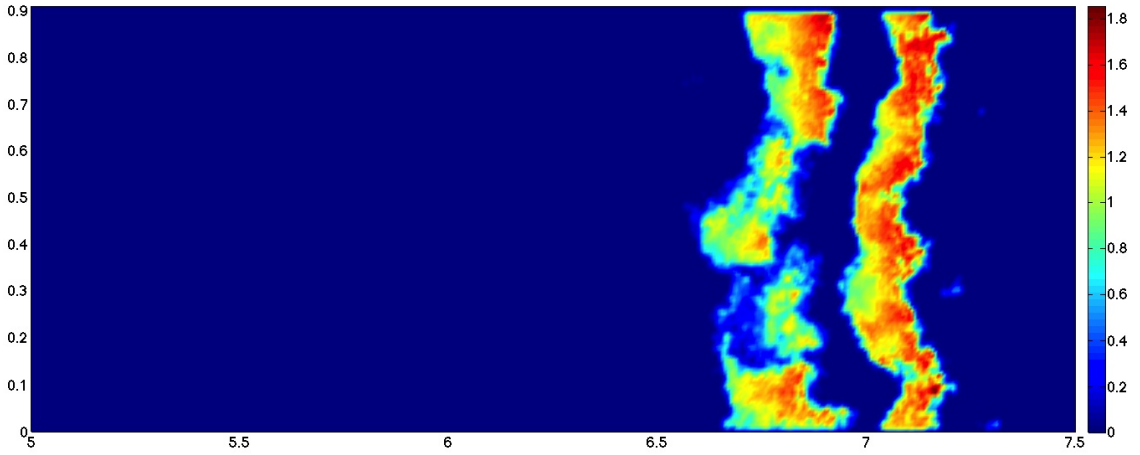

Figure 9: Streamwise velocity on a plane that is parallel to the x-y plane, at the position of $z = 0.42m$, and at time = 4 s, showing the variation of streamwise velocity over the width of the tank

and vertical vorticity to streamwise vorticity respectively. Term one and two of equation 12 ($\omega_x \frac{\partial w}{\partial x}$, $\omega_y \frac{\partial w}{\partial y}$) also have large values, which are associated to vortex turning from streamwise vorticity to vertical vorticity and spanwise vorticity to vertical vorticity respectively. Term one of equation 11 and term three of 12 ($\omega_x \frac{\partial u}{\partial x}$ and $\omega_z \frac{\partial w}{\partial z}$), which are associated to vortex stretching in x and z directions, have smaller values.

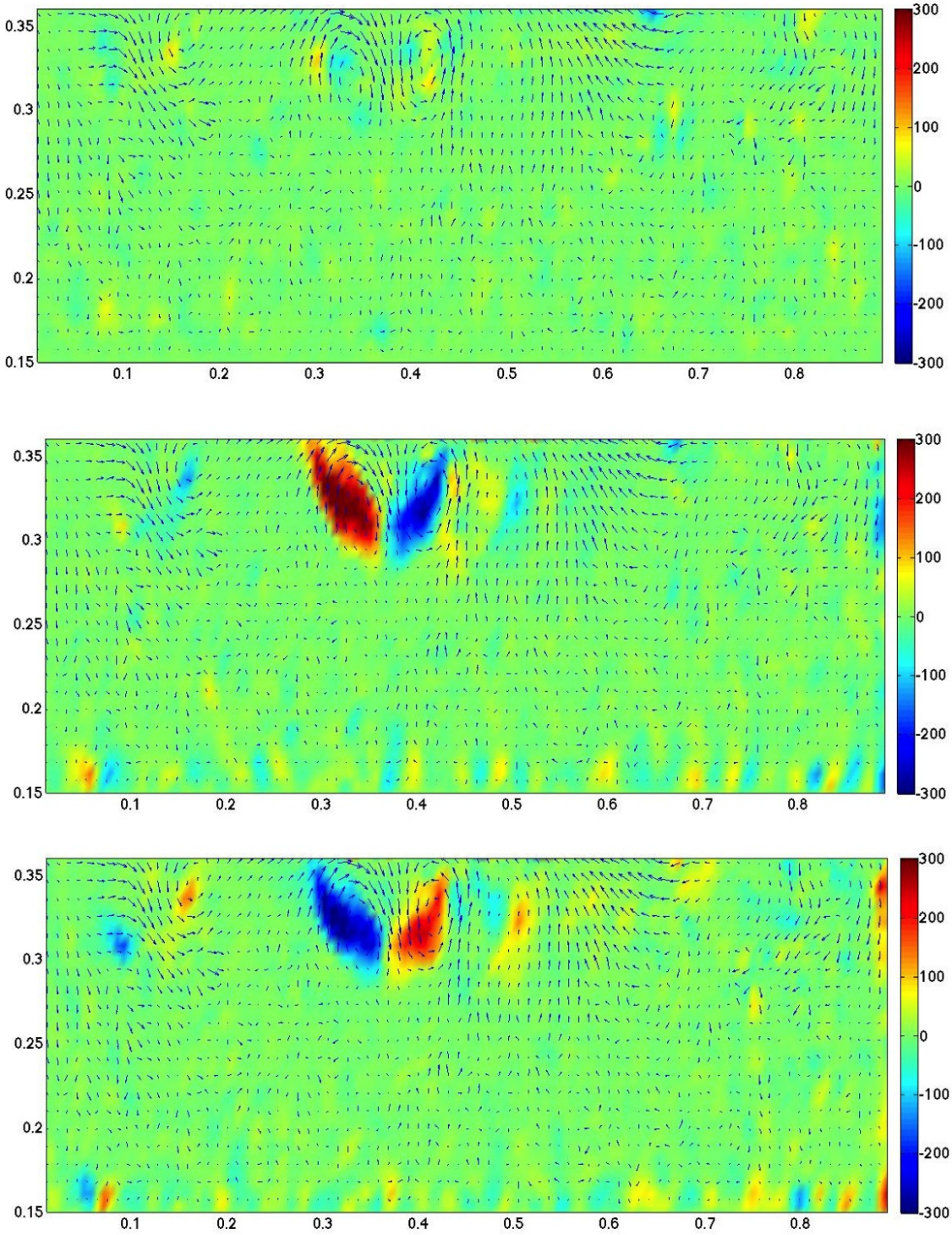

Figure 10: Vorticity equation terms. From top to bottom: $\omega_x \frac{\partial u}{\partial x}$, $\omega_y \frac{\partial u}{\partial y}$, $\omega_z \frac{\partial u}{\partial z}$, $\omega_x \frac{\partial w}{\partial x}$, $\omega_y \frac{\partial w}{\partial y}$, $\omega_z \frac{\partial w}{\partial z}$

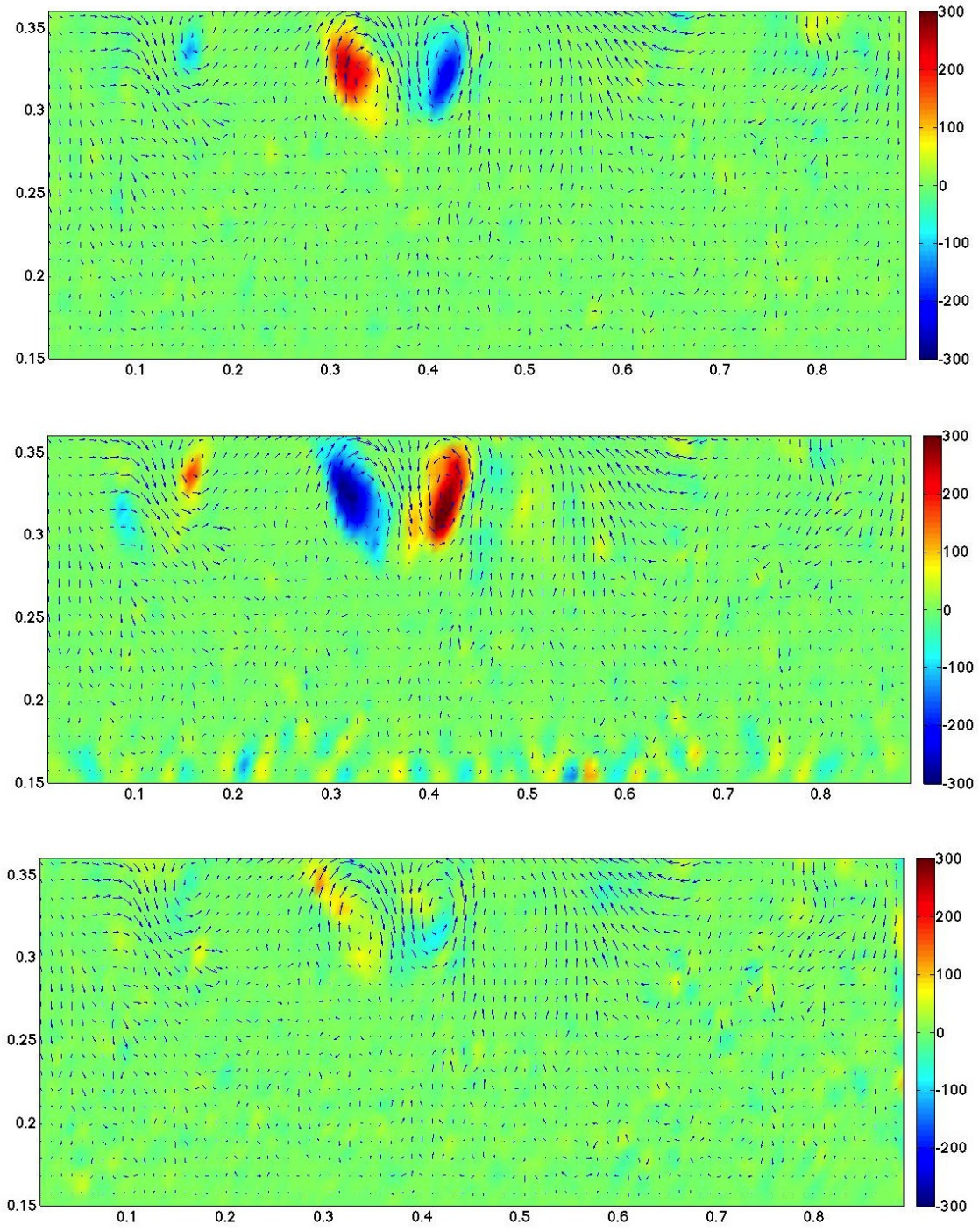

Figure 10: (Continued)Vorticity equation terms. From top to bottom: $\omega_x \frac{\partial u}{\partial x}$, $\omega_y \frac{\partial u}{\partial y}$, $\omega_z \frac{\partial u}{\partial z}$, $\omega_x \frac{\partial w}{\partial x}$, $\omega_y \frac{\partial w}{\partial y}$, $\omega_z \frac{\partial w}{\partial z}$

CONCLUSION

A three-dimensional numerical method called Smoothed Particle Hydrodynamics is used to model a broken spilling water wave and the resulting three-dimensional vortex structures. The numerical results of wave height profiles and surface evolution agree well with the experimental results of Ting (2006). Three dimensional reversed horseshoe vortex structures are detected at the back of the broken wave, which were

previously observed as obliquely descending eddies. The counter-rotating legs of the reversed horseshoe structures correspond to the obliquely descending eddies. The physical mechanism of the generation and evolution of reversed horseshoe coherent structures were discussed by analyzing the vorticity equations and the vortex stretching and vortex turning terms.

References

[1] E. D. Christensen *Large eddy simulation of spilling and plunging breakers*, Coastal Engineering, 53, 463-485, 2006.

[2] R. A. Dalrymple, O. Knio, D. T. Cox, M. Gómez-Gesteira, and S. Zou, *Using a Lagrangian particle method for deck overtopping*, Proc. of Waves, ASCE., 1082-1091, 2002.

[3] R. A. Dalrymple and B. D. Rogers, *Numerical modeling of water waves with SPH method*, Coastal Engineering, 53, 141-147, 2006.

[4] R. J. Farahani, R. A. Dalrymple, A. Hérault, G. Bilotta,*Three-Dimensional SPH Modeling of a Bar/Rip Channel System*, Journal of Waterway, Port, Coastal, and Ocean Engineering, 140, pp. 82-99, 2014.

[5] R. A. Gingold, J. J. Monaghan, *Smoothed particle hydrodynamics: Theory and application to non-spherical stars*, Monthly notices of the royal astronomical society, 181, 375-389,1977.

[6] D. Goring, F. Raichlen, *The generation of long waves in the laboratory*, Coastal Engineering, 763-783, 1980.

[7] M. Gómez-Gesteira,and R. A. Dalrymple, *Using a three-dimensional Smoothed Particle Hydrodynamics method for wave impact on a tall structure* Journal of Waterway, Port, Coastal and Ocean Engineering, ASCE, 130(2) 63-69,2004.

[8] A. Hérault, G. Bilotta, A. Vicari, E. Rustico, and C. D. Negro, *Numerical simulation of lava flow using a GPU SPH model*, Annals of Geophysics, 54(5), 600-620, 2011.

[9] A. K. M. Hussain, *Coherent structures and turbulence*, Journal of Fluid Mechanics, 173., 303-356, 1986.

[10] J. Jeong, and F. Hussain, *On the identification of a vortex*, Journal of Fluid Mechanics, 285, 69-94, 1994.

[11] J. Kim, and P. Moin, *The structure of the vorticity field in turbulent channel flow. Part 2. Study of ensemble-averaged fields*, Journal of Fluid Mechanics, 162, 339-363, 1986.

[12] J. J. Monaghan, *Simulating free surface flows with SPH*, Computational Physics, 110, 399-406,1994.

[13] J. J. Monaghan and A. Kos, *Solitary waves on a certain beach*, Journal of Waterway, Port, Coastal and Ocean Engineering, 145-154, 1999.

[14] J. J. Monaghan, A. Kos, and N. Issa, *Fluid motion generated by impact*, Journal of Waterway, Port, Coastal and Ocean Engineering, 129(6) 250-259, 2003.

[15] K. Nadaoka, M. Hino, and Y. Koyano, *Structure of the turbulent flow field under breaking waves in the surf zone*, Journal of Fluid Mechanics, 204, 359-387, 1989.

[16] F. C. K. Ting and J. T. Kirby, *Observation of undertow and turbulence in a laboratory surf zone*, Coastal Engineering, 24, 52-80,1994.

[17] F. C. K. Ting *Large-scale turbulence under a solitary wave*, Coastal Engineering, 53, 441-462, 2006.

[18] Y. Watanabe and H. Saeki, *Three-dimensional large eddy simulation of breaking waves*, Coastal Engineering, 41, 281-301, 1999.

[19] D. Yang, L. Shen, *Characteristics of coherent vortical structures in turbulent flows over progressive surface waves*, Physics of Fluids, 21, 125106, 1-23, 2009.